

Article

# Organically Templated Layered Uranyl Molybdate $[\text{C}_3\text{H}_9\text{NH}^+]_4[(\text{UO}_2)_3(\text{MoO}_4)_5]$ Structurally Based on Mineral-Related Modular Units

Evgeny Nazarchuk <sup>1,\*</sup>, Dmitri Charkin <sup>2</sup>, Oleg Siidra <sup>1,3</sup>  and Stepan Kalmykov <sup>2</sup>

<sup>1</sup> Department of Crystallography, Saint-Petersburg State University, University emb. 7/9, 199034 St. Petersburg, Russia; siidra@mail.ru

<sup>2</sup> Department of Chemistry, Moscow State University, GSP-1, 119991 Moscow, Russia; d.o.charkin@gmail.com (D.C.); stepan@radio.chem.msu.ru (S.K.)

<sup>3</sup> Kola Science Center, Russian Academy of Sciences, 184200 Apatity, Russia

\* Correspondence: e\_nazarchuk@mail.ru; Tel.: +7-921-156-14-79

Received: 5 July 2020; Accepted: 24 July 2020; Published: 25 July 2020



**Abstract:** A new organically templated uranyl molybdate  $[\text{C}_3\text{H}_9\text{NH}^+]_4[(\text{UO}_2)_3(\text{MoO}_4)_5]$  was prepared by a hydrothermal method at 220 °C. The compound is monoclinic, *Cc*,  $a = 16.768(6)$ ,  $b = 20.553(8)$ ,  $c = 11.897(4)$  Å,  $\beta = 108.195(7)$ ,  $V = 3895(2)$  Å<sup>3</sup>,  $R_1 = 0.05$ . The crystal structure is based upon  $[(\text{UO}_2)_3(\text{MoO}_4)_5]^{4-}$  uranyl molybdate layers. The isopropylammonium cations are located in the interlayer. The layers in the structure of  $[\text{C}_3\text{H}_9\text{NH}^+]_4[(\text{UO}_2)_3(\text{MoO}_4)_5]$  are considered as modular architectures. Topological analysis of layers with  $\text{UO}_2:\text{TO}_4$  ratio of 3:5 ( $T^{\text{VI}} = \text{S, Cr, Se, Mo}$ ) was performed. Modular description is employed to elucidate the relationships between different structural topologies of  $[(\text{UO}_2)_3(\text{TO}_4)_5]^{4-}$  layers and inorganic uranyl-based nanotubules. The possible existence of uranyl molybdate nanotubules is discussed.

**Keywords:** uranyl molybdates; uranyl sulfates; uranyl selenates; crystal structure; layered structures; minerals; nanotubules

## 1. Introduction

Investigations of natural and synthetic compounds of hexavalent uranium are important both for materials science and mineralogy. Uranium minerals are important constituents of oxidation zones of uranium deposits [1,2]. The development of the nuclear industry also requires further investigations in the area of safe nuclear waste management [3]. The latter requires proper understanding of phase formation processes, relationships between chemical compositions, crystal structures, and properties of the compounds formed. Of particular interest are both the chemical nature of the possible secondary phases and their interactions with the geological environment [4].

In the last two decades, particular attention has been paid to the hexavalent uranium (uranyl) compounds containing organic moieties, which are important for lanthanide/actinide separation. Common among these are the hybrid materials wherein the organic molecules are directly coordinated to the uranyl cation as ligands [5,6]. The templated structures based on weakly bonded organic and inorganic parts are less numerous [7] but exhibit essentially larger structural diversity of inorganic motifs.

The uranium compounds are formed during various steps of the nuclear cycle and present in the nuclear waste [3]. They accumulate various nuclides, thus preventing their migration into the environment [4]. The composition of nuclear waste is extremely complex and can contain both newly formed phases, as well as products of interaction between the fuel and container material, as well as with geological environment. The molybdenum isotopes (<sup>95</sup>Mo, <sup>97</sup>Mo, <sup>98</sup>Mo and <sup>100</sup>Mo), formed

during the fission process, are relatively stable and accumulate in the waste fuel. Topologically similar and even isostructural compounds are also known in the chemistry of pentavalent neptunium [7].

Though the natural and synthetic uranyl compounds are generally formed under essentially different conditions, their crystal structures demonstrate topological relationships [8]. Of more than 300 primary and secondary uranium minerals known to date (<http://rruff.info/ima>), the latter demonstrate the expected richer structural chemistry wherein uranium most commonly forms a linear uranyl cation coordinated by four, five, or six ligands in the equatorial plane. The coordination polyhedra can share only edges, only corners, or both edges and corners between each other or also with tetrahedral polyhedra of oxyanions. The group of compounds structurally based on exclusively corner sharing between  $UO_n$  polyhedra and  $TO_4$  ( $T^{VI} = S, Cr, Se, Mo$ ) tetrahedra is represented in the secondary minerals. Their structures exhibit two types of 0D, four 1D, and four 2D complexes (Figure 1).

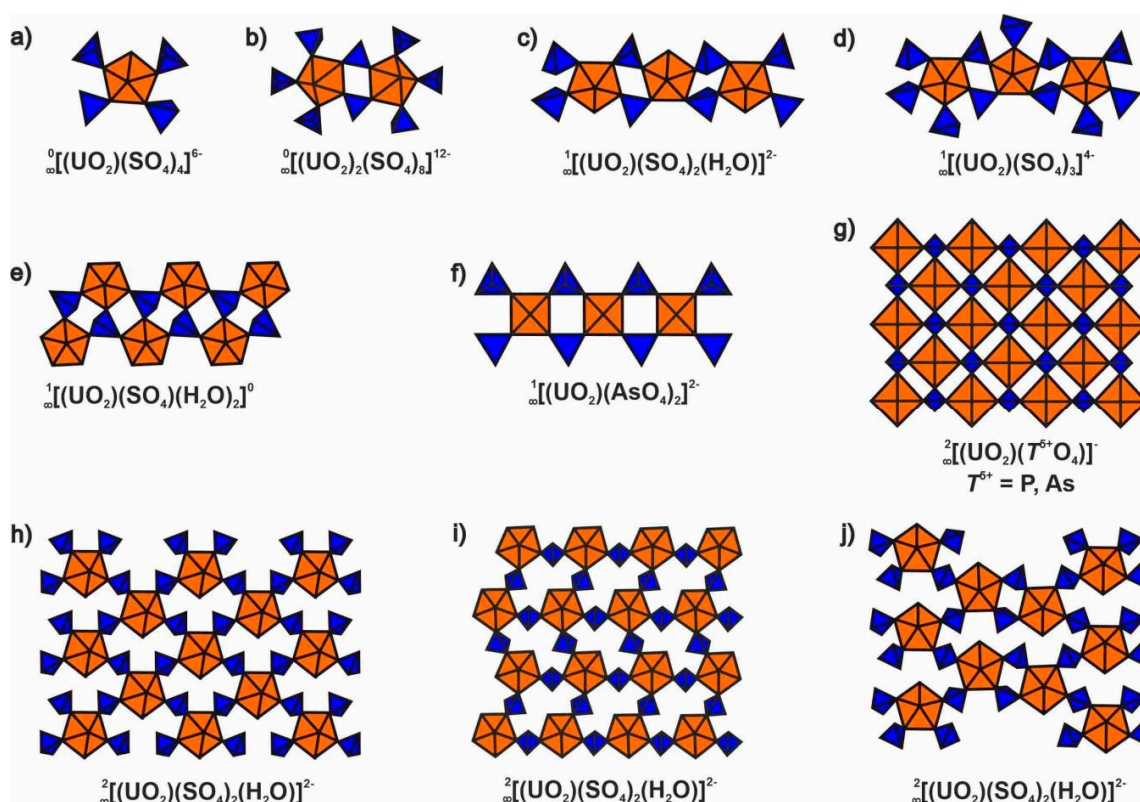


**Figure 1.** Heteropolyhedral complexes with corner sharing only between  $UO_n$  bipyramids and  $TO_4$  tetrahedra in the mineral crystal structures: (a) belakovskiite, (b) bluelizardite, (c) bobcookite, (d) meisserite, (e) shumwayite, (f) walpurgite, (g) autunite, (h) straßmannite, (i) wetherillite and (j) beshtauite.

The 0D complexes are observed in the sulfate minerals belakovskiite,  $Na_7(UO_2)(SO_4)_4(SO_3OH) \cdot 3H_2O$  [9] and bluelizardite,  $Na_7(UO_2)(SO_4)_4Cl \cdot 2H_2O$  [10], which are the secondary products of uraninite weathering; both species have been found in the Blue Lizard mine, San Juan, UT, USA. Though a large number of natural uranyl sulfates has been described [11], the complexes observed in belakovskiite (Figure 1a) and bluelizardite (Figure 1b) are yet unique.

The same locality also has bobcookite,  $NaAl(UO_2)_2(SO_4)_4 \cdot 18H_2O$  [12], fermiite,  $Na_4(UO_2)(SO_4)_3 \cdot 3H_2O$ , and oppenheimerite,  $Na_2(UO_2)(SO_4)_2 \cdot 3H_2O$  [13], whose structures are comprised of  $[(UO_2)(SO_4)_2(H_2O)]^{2-}$  chains (Figure 1c). This topology is common for synthetic uranyl sulfates, selenates, and chromates [14]. They are also present in the structures of rietveldite,  $Fe(UO_2)(SO_4)_2 \cdot 5H_2O$  [15] and svornostite,  $K_2Mg[(UO_2)(SO_4)_2]_2 \cdot 8H_2O$  [16]. The chains observed in the structure of meisserite,  $Na_5(UO_2)(SO_4)_3(SO_3OH) \cdot H_2O$  [17] can be derived from  $[(UO_2)(SO_4)_2(H_2O)]^{2-}$  chains [18] via the addition

of a protonated sulfate tetrahedron (Figure 1d). The structure of shumwayite,  $((\text{UO}_2)(\text{SO}_4)(\text{H}_2\text{O})_2)_2 \cdot \text{H}_2\text{O}$  [19] is formed by association of  $[(\text{UO}_2)(\text{SO}_4)(\text{H}_2\text{O})_2]$  chains (Figure 1e) and water via hydrogen bonding. In the structures of deloryite,  $\text{Cu}_4(\text{UO}_2)(\text{MoO}_4)_2(\text{OH})_6$  [20], walpurgite,  $(\text{BiO})_4(\text{UO}_2)(\text{AsO}_4)_2 \cdot 2\text{H}_2\text{O}$  [21], and orthowalpurgite,  $(\text{BiO})_4(\text{UO}_2)(\text{AsO}_4)_2 \cdot 2\text{H}_2\text{O}$  [22], the  $[(\text{UO}_2)(\text{TO}_4)_2]^{2-}$  chains are comprised of  $\text{UO}_6$  tetragonal bipyramids and  $\text{TO}_4$  tetrahedra sharing vertices (Figure 1f). Their association leads to the formation of autunite-type layers (Figure 1g) [23].

A large number of uranium minerals with a common formula  $A^{n+}[(\text{UO}_2)(\text{TO}_4)](\text{H}_2\text{O})_m X_k$  adopt the structures based on autunite-related  $[(\text{UO}_2)(\text{T}^{\text{V}}\text{O}_4)]^-$  layers. Therein,  $A$  may stand for a single, double, or even triple-charged cation while  $T$  is P or As, and  $X$  is generally F or OH. The layers observed in the structures of magnesiolydetite,  $\text{Mg}(\text{UO}_2)(\text{SO}_4)_2 \cdot 11\text{H}_2\text{O}$ , straßmannite,  $\text{Al}(\text{UO}_2)(\text{SO}_4)_2 \text{F} \cdot 16\text{H}_2\text{O}$  [24], geschieberite,  $\text{K}_2(\text{UO}_2)(\text{SO}_4)_2 \cdot 2\text{H}_2\text{O}$  [25], and leydetite,  $\text{Fe}(\text{UO}_2)(\text{SO}_4)_2 \cdot 11\text{H}_2\text{O}$  [26] are topologically identical (Figure 1h). Therein, four out of five equatorial vertices of uranium polyhedra are occupied by oxygen atoms of sulfate tetrahedra while the fifth is occupied by a water molecule; all such vertices are similarly oriented in the layer plane. The layers in the structure of wetherillite,  $\text{Na}_2\text{Mg}(\text{UO}_2)_2(\text{SO}_4)_4 \cdot 18\text{H}_2\text{O}$  [12], differ in that the vertices occupied by water molecules exhibit two positions (Figure 1i). Yet another layered arrangement is formed by vertex-sharing  $\text{UO}_6(\text{H}_2\text{O})$  and  $\text{SO}_4$  moieties (Figure 1j) in the structure of beshtauite,  $(\text{NH}_4)_2(\text{UO}_2)(\text{SO}_4)_2 \cdot 2\text{H}_2\text{O}$  [27]. The topology of this layer is similar to that of goldichite,  $\text{KFe}(\text{SO}_4)_2 \cdot 4\text{H}_2\text{O}$  [28].

The structural diversity of natural and synthetic compounds is mostly governed by their formation conditions, including the acidity/basicity and the mechanism of crystallization. The majority of the minerals discussed above have been found on the walls of abandoned mines [10]. They crystallize upon evaporation under almost invariable temperature but decreasing pH. These conditions are expected to affect the structural outcome. The oxidation zones are formed under conditions changing from basic to weakly acidic [1]. Interestingly, in most structures of these minerals,  $\text{UO}_n$  bipyramids and  $\text{TO}_4$  tetrahedra preferably involve corner sharing only.

Essentially richer structural chemistry with similar architecture is observed for synthetic uranyl compounds, particularly for those that are organically templated and formed in acidic environments. Hydrogen-bonded motifs are particularly common in organically templated synthetic uranyl compounds. Most synthetic protocols, using evaporation techniques, for uranyl compounds with tetrahedral anions employ essentially acidic media (pH = 2–4 and below) [29–32].

Hence, the minerals formed upon solution evaporation on the mine walls, as well as synthetic compounds, also formed by evaporation of acidic solutions, demonstrate topologically similar crystal structures. This indicated that studies of synthetic compounds, their topological variability and structural peculiarities are of essential importance.

Among both natural and synthetic uranium compounds, the largest topological diversity is exhibited by the structures of compounds containing tetrahedral  $\text{TO}_4^{2-}$  anions ( $T^{\text{VI}} = \text{S}, \text{Cr}, \text{Se}, \text{Mo}$ ) [14]. Despite chemical differences, they commonly demonstrate topologically identical structural motifs. Note that crystal chemistry of  $\text{Mo}^{\text{VI}}$  compounds is more complex due to its flexible coordination environments.

In this paper, we report the synthesis and structure of new uranyl molybdate  $[\text{C}_3\text{H}_9\text{NH}^+]_4[(\text{UO}_2)_3(\text{MoO}_4)_5]$  (1). Its structure is based upon  $[(\text{UO}_2)_3(\text{MoO}_4)_5]^{4-}$  uranyl molybdate layers, which may be considered as a precursor for nanotubule formation.

## 2. Materials and Methods

**Synthesis.** Crystals of  $[\text{C}_3\text{H}_9\text{NH}^+]_4[(\text{UO}_2)_3(\text{MoO}_4)_5]$  (1) were synthesized from a solution of 0.1 g of  $(\text{UO}_2)(\text{NO}_3)_2 \cdot 6\text{H}_2\text{O}$  (Vekton, 99.7%), 0.0576 g of  $\text{MoO}_3$  (Vekton, 99.7%), 0.01 mL of isopropylamine (Aldrich, 99.5%) and 0.053 g of HCl in 5 mL of  $\text{H}_2\text{O}$  (with an approximate U:Mo:isopropylamine:HCl: $\text{H}_2\text{O}$  molar gel ratio of 3:5:8:15:1550). The solution was placed in a Teflon-lined Parr reaction vessel and heated to 220 °C for 36 h (6 °C/h), followed by slow cooling to ambient

temperature. The cooling rate was 2 °C/h. The crystals occur as aggregates of greenish-yellow transparent plates up to 0.2 mm in maximum dimension.

*Single-crystal studies.* A single crystal was attached to glass fiber using an epoxy resin and mounted on a Bruker SMART APEX II DUO diffractometer (Bruker, Karlsruhe, Germany) equipped with a micro-focus X-ray tube utilizing MoK $\alpha$  radiation. The experimental data set was collected at 100 K. Unit cell parameters were calculated using least-squares fits. Structure factors were derived using APEX 2 after introducing the required corrections. The structure was solved using direct methods. Further details are collected in Table 1. The final model includes site coordinates and anisotropic thermal parameters for all atoms except hydrogens, which were localized using AFIX command in calculated positions ( $d(\text{C-H}, \text{N-H}) = 1.00 \text{ \AA}$ ). The data are deposited in CCDC under Entry No. 2014144. Selected interatomic distances are given in Table 2.

**Table 1.** Crystallographic data and refinement parameters for  $[\text{C}_3\text{H}_9\text{NH}^+]_4[(\text{UO}_2)_3(\text{MoO}_4)_5]$ . Experiments were carried out at 100 K with Mo K $\alpha$  radiation on a Bruker Smart DUO, CCD.

Space Group	Cc
$a(\text{\AA})$	16.768 (6)
$b(\text{\AA})$	20.553 (8)
$c(\text{\AA})$	11.897 (4)
$\beta, ^\circ$	108.195 (7)
$V(\text{\AA}^3)$	3895 (2)
$D_x$	3.155
$\theta \text{ max } (^\circ)$	1.62–28.00
No. of measured, independent reflections	9176/7160
$R_{\text{int}}$	0.0694
$R_{\text{sigma}}$	0.1213
$wR_1$	0.1182
$R_1$	0.0520
S	0.944
CCDC	2014144

**Table 2.** Selected bond lengths  $\text{\AA}$  in the structure of 1.

<b>U1-O3</b>	<b>1.765 (13)</b>	<b>U2-O1</b>	<b>1.724 (15)</b>	<b>U3-O4</b>	<b>1.729 (14)</b>
U1-O5	1.796 (12)	U2-O2	1.767 (15)	U3-O8	1.791 (13)
<b>&lt;Ur1-O&gt;</b>	<b>1.780</b>	<b>&lt;Ur2-O&gt;</b>	<b>1.745</b>	<b>&lt;Ur3-O&gt;</b>	<b>1.760</b>
U1-O12	2.299 (12)	U2-O13	2.304 (11)	U3-O26	2.287 (14)
U1-O18	2.367 (11)	U2-O9	2.320 (10)	U3-O24	2.332 (12)
U1-O22	2.371 (11)	U2-O23	2.372 (11)	U3-O20	2.369 (10)
U1-O16	2.408 (10)	U2-O17	2.375 (11)	U3-O11	2.391 (11)
U1-O7	2.437 (11)	U2-O6	2.583 (12)	U3-O19	2.497 (12)
<b>&lt;U1-O<sub>eq</sub>&gt;</b>	<b>2.376</b>	<b>&lt;U2-O<sub>eq</sub>&gt;</b>	<b>2.391</b>	<b>&lt;U3-O<sub>eq</sub>&gt;</b>	<b>2.375</b>
Mo1-O21	1.688 (12)	Mo2-O10	1.691 (15)	Mo3-O15	1.698 (13)
Mo1-O22	1.735 (11)	Mo2-O6	1.742 (13)	Mo3-O17	1.774 (10)
Mo1-O9	1.770 (11)	Mo2-O16	1.766 (10)	Mo3-O18	1.779 (11)
Mo1-O12	1.776 (12)	Mo2-O11	1.798 (11)	Mo3-O7	1.789 (11)
<b>&lt;Mo1-O&gt;</b>	<b>1.742</b>	<b>&lt;Mo2-O&gt;</b>	<b>1.749</b>	<b>&lt;Mo3-O&gt;</b>	<b>1.760</b>
Mo4-O14	1.703 (13)	Mo5-O25	1.666 (16)		
Mo4-O19	1.761 (12)	Mo5-O26	1.702 (14)		
Mo4-O23	1.761 (11)	Mo5-O24	1.765 (13)		
Mo4-O20	1.795 (11)	Mo5-O13	1.767 (12)		
<b>&lt;Mo4-O&gt;</b>	<b>1.755</b>	<b>&lt;Mo5-O&gt;</b>	<b>1.725</b>		

### 3. Results

The structure of **1** (Figure 2a) contains three symmetrically independent uranium atoms each forming the uranyl cation ( $\langle \text{U-O} \rangle = 1.780, 1.745, 1.760 \text{ \AA}$ , for U1, U2, U3, respectively).  $(\text{UO}_2)^{2+}$  cations (*Ur*) are each coordinated by five oxygen atoms in the equatorial plane ( $\langle \text{Ur-O}_{eq} \rangle = 2.376, 2.391, 2.375 \text{ \AA}$ , respectively). Five symmetrically unique molybdenum atoms form  $(\text{MoO}_4)^{2-}$  tetrahedra ( $\langle \text{Mo-O} \rangle = 1.742, 1.749, 1.760, 1.755, 1.725 \text{ \AA}$ , respectively).

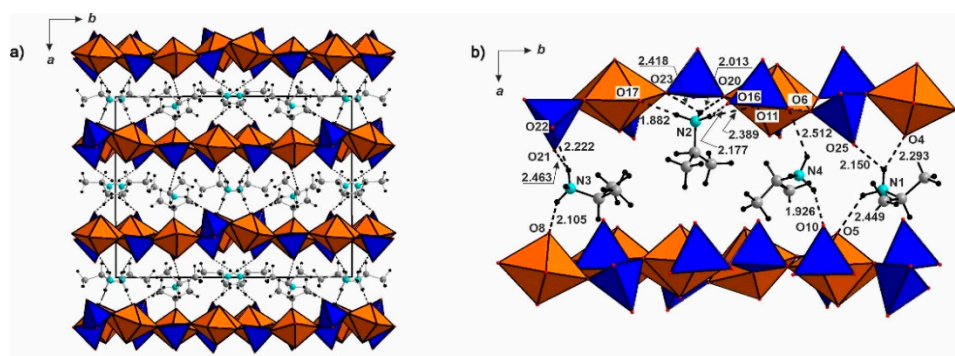


**Figure 2.** (a) General projection of the crystal structure of **1** along the *c* axis and (b) hydrogen bonding with isopropylamine molecules in the interlayer ( $\text{UO}_7$  bipyramids = orange,  $\text{MoO}_4$  = blue, H = black, C = grey).

The bond valence sums for U and Mo were calculated using parameters given in [33]: 5.98, 6.17 and 6.14 for U1, U2 and U3, and 6.12, 6.02, 5.86, 5.93 and 6.39 for Mo1, Mo2, Mo3, Mo4 and Mo5, respectively. These values are in agreement with the reference data except for the somewhat overbonded Mo5 centering a strongly distorted tetrahedron (Mo-O distances to O24, O13, O26 and O25 are  $1.765(13) \text{ \AA}$ ,  $1.767(12) \text{ \AA}$ ,  $1.702(14) \text{ \AA}$ , and  $1.666(16) \text{ \AA}$ ). This distortion is likely due to a strong N-H $\cdots$ O hydrogen bond ( $d(\text{N1-O25}) = 2.150 \text{ \AA}$ ) (Figure 2b).

The  $\text{UO}_7$  and  $\text{MoO}_4$  polyhedra share corners to form the  $[(\text{UO}_2)_3(\text{MoO}_4)_5]^{4-}$  layers (Figure 3a). Protonated molecules of isopropylamine are located in the interlayer and connected to the layers via hydrogen bonding (Figure 2b). The  $[(\text{UO}_2)_3(\text{MoO}_4)_5]^{4-}$  layer topology has been described earlier in the structures of uranyl molybdates [34], selenates [35] and chromates [36]. The orientation matrix for the terminal oxygen atoms of the molybdate tetrahedra in **1** is given in Figure 3b. A compound with the same chemical composition, same graph of the layers (Figure 3c), but with the different orientation matrix for the terminal oxygen atoms of the molybdenum tetrahedra was found in the structure of  $[\text{C}_3\text{N}_2\text{H}_{12}](\text{H}_3\text{O})_2[(\text{UO}_2)_3(\text{MoO}_4)_5]$  [34]. According to the definition given in [37], such layers are orientation geometric isomers. Thus, the orientation matrix for the  $[(\text{UO}_2)_3(\text{MoO}_4)_5]^{4-}$  layer in **1** has not been observed before.

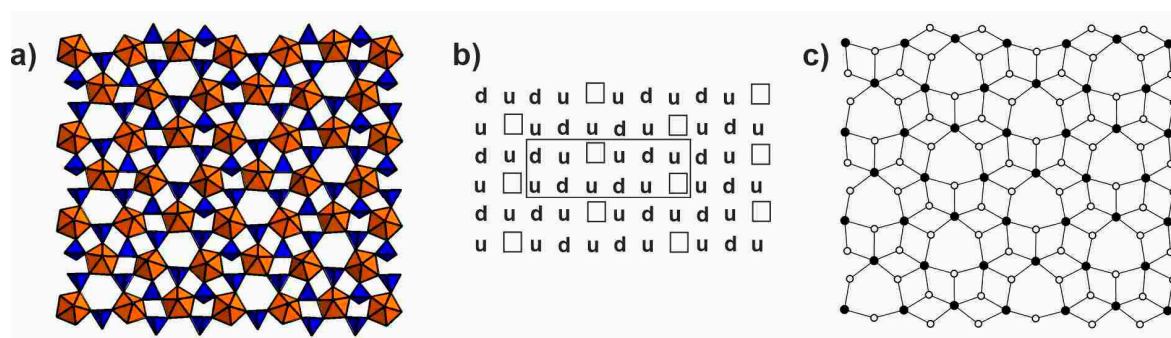


**Figure 3.** (a) The  $[(\text{UO}_2)_3(\text{MoO}_4)_5]^{4-}$  layer in the structure of **1**; (b) orientation matrix of the terminal oxygen atoms (non-shared vertices of  $\text{MoO}_4$  tetrahedra), and (c) the corresponding graph.

There are three common approaches to the description of the structural topology of uranium minerals and synthetic compounds: anionic topologies, graphs, and modular description. In [38], the latter approach was applied to demonstrate that structures of some uranyl selenates may be obtained via assembly of  $[(\text{UO}_2)_2(\text{SeO}_4)_4(\text{H}_2\text{O})_4]^{4-}$  modules. The layers in the structure of  $[\text{Co}(\text{H}_2\text{O})_6]_3(\text{UO}_2)_5(\text{SO}_4)_8(\text{H}_2\text{O})\cdot\text{H}_2\text{O}$  can also be viewed as a modular arrangement formed by the assembly of chains [39]. A modular approach was also applied to the description of some uranyl chromates, sulfates and selenates [40,41]. It was shown [41] that layers with the ratio  $\text{UO}_2:\text{TO}_4 = 2:3$  can be obtained by the association of two types of fundamental chains.

The  $[(\text{UO}_2)_3(\text{MoO}_4)_5]^{4-}$  layer in **1** (Figure 4) can be also described as consisting of several modules, i.e., fundamental chains C1, C2, C'1. The C1 and C'1 chains are related by a mirror plane. In C1 chains,  $(\text{U1O}_2)\text{O}_5$  and  $(\text{U2O}_2)\text{O}_5$  bipyramids share vertices with  $\text{Mo1O}_4$  and  $\text{Mo2O}_4$  tetrahedra, to form the  $[(\text{UO}_2)_2(\text{MoO}_4)_4]^{4-}$  complexes linked via additional  $\text{Mo3O}_4$  species. C2 chains are formed from two  $(\text{U3O}_2)\text{O}_5$  bipyramids and  $\text{Mo4O}_5$  and  $\text{Mo5O}_5$  species. The chains are stacked in the following sequence ...C1C2C'1C1C2C'1 ...

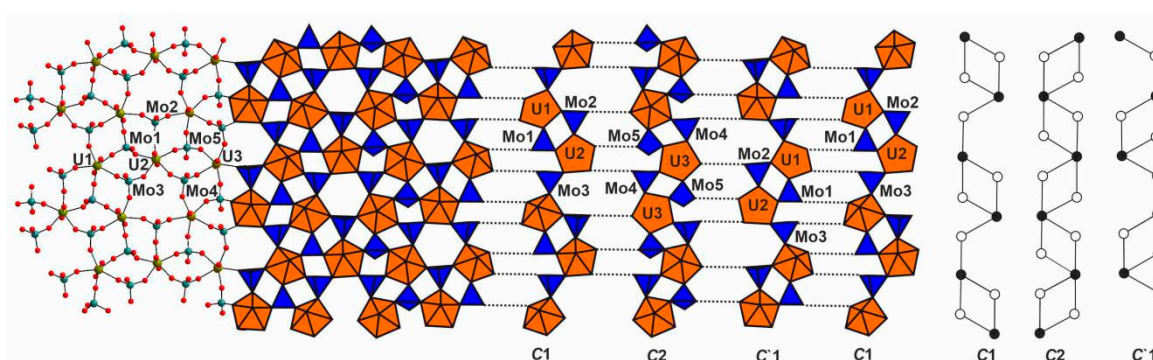


Figure 4. The topology of  $[(\text{UO}_2)_3(\text{MoO}_4)_5]^{4-}$  layer in **1**.

Three topologies of  $\text{UO}_2:\text{TO}_4 = 3:5$  layers [14] are known to date. Two of them are represented in Figure 5. In all cases, the layers can be described as alternations of chains.

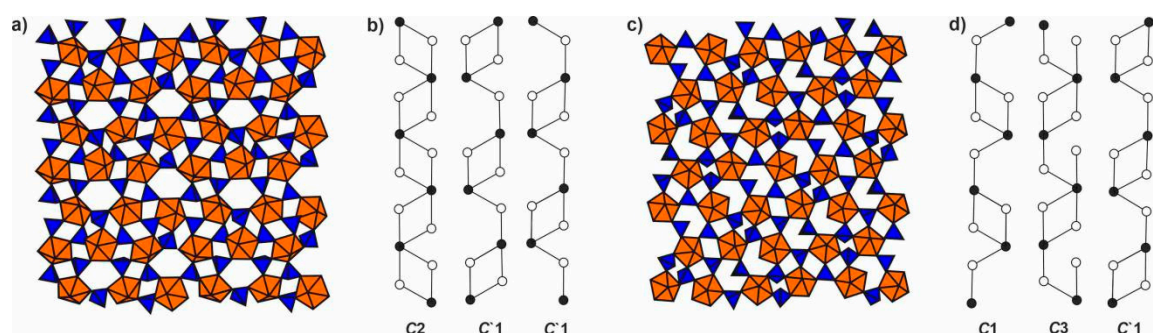


Figure 5. (a) Structure of the  $[(\text{UO}_2)_3(\text{TO}_4)_5]^{4-}$  layers in  $\text{Zn}_2((\text{UO}_2)_3(\text{SeO}_4)_5)\cdot 17(\text{H}_2\text{O})$  and (c)  $\text{Rb}_2((\text{UO}_2)_2(\text{SeO}_4)_3(\text{H}_2\text{O})_2)\cdot 4(\text{H}_2\text{O})$  and (b, d) their split into fundamental chains.

The  $[(\text{UO}_2)_3(\text{TO}_4)_5]^{4-}$  layers in the structure of  $\text{Zn}_2((\text{UO}_2)_3(\text{SeO}_4)_5)\cdot 17(\text{H}_2\text{O})$  (Figure 5a) are constructed in a way similar to the layers in **1**. They are formed by combination of C2 and C'1 chains (Figure 5b) in a ... C2C'1C'1C2C'1C'1 ... sequence. The layers in the structure of  $\text{Rb}_2((\text{UO}_2)_2(\text{SeO}_4)_3(\text{H}_2\text{O})_2)\cdot 4(\text{H}_2\text{O})$  (Figure 5c) exhibit a different topology and are formed from three types of chains: C1, C3, and C'1 (Figure 5d). The C3 chain can be obtained from C2 by the removal of one link between the nodes in every second four-membered cycle.

## 4. Discussion

### 4.1. Structural Topology of Nanotubes Is Uranyl Oxysalts

Four uranyl compounds with nanotubular (NT) motifs formed by corner sharing between  $UO_7$  bipyramids and  $TO_4$  tetrahedra have been described to date: three uranyl-selenates [42,43] and one uranyl-sulfate [44]. Nanotubes differ both in the diameter and structural topology of their walls. The compounds  $K_5(UO_2)_3(SeO_4)_5(NO_3) \cdot 3.5(H_2O)$  and  $(H_3O)_2K[(H_3O)@([18]crown-6)][(UO_2)_3(SeO_4)_5] \cdot 4H_2O$  are based on identical nanotubes  $[(UO_2)_3(SeO_4)_5]^{4-}$  (Figure 6a). Their outer diameter is 17 Å and the inner one (defined as the distance between the opposite closest oxygen atoms) is 7.4 Å. In the structure of  $(C_4H_{12}N)_{14}[(UO_2)_{10}(SeO_4)_{17}(H_2O)]$  the  $[(UO_2)_{10}(SeO_4)_{17}(H_2O)]^{14-}$  nanotubes are elliptical with dimension  $25 \times 23$  Å (inner diameter is 15.3 Å) (Figure 6c). The size of  $[(UO_2)_6(SO_4)_{10}]^{8-}$  nanotubes (Figure 6b) in the structure of  $Na(C_8H_{10}NO_2)_7[(UO_2)_6(SO_4)_{10}] \cdot 3.5H_2O$  [44] is intermediate ( $14 \times 22$  Å, inner diameter is 13.5 Å).

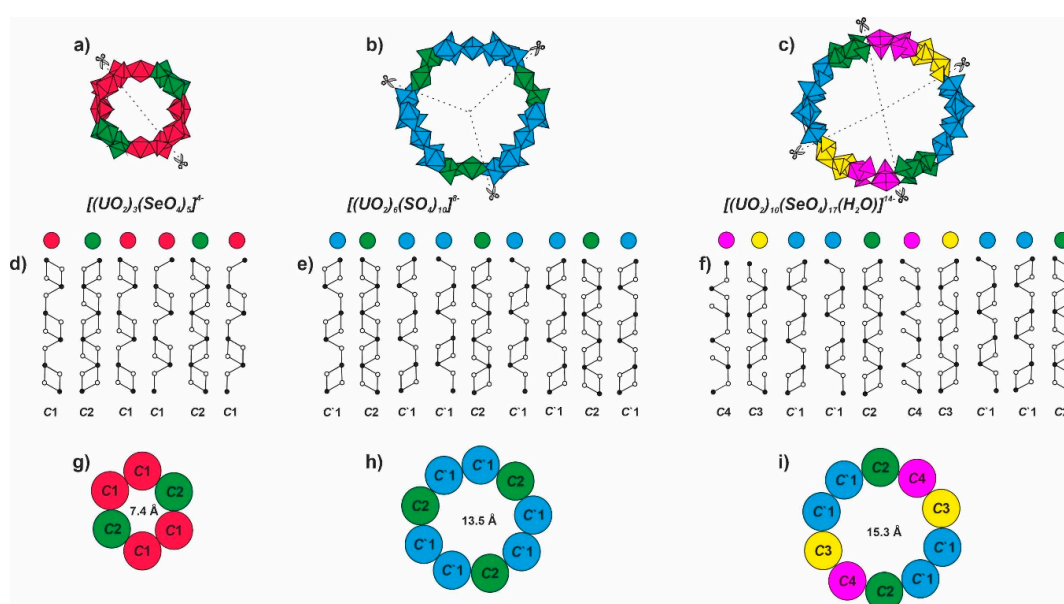


**Figure 6.** (a) Known uranyl-based nanotubes in  $K_5(UO_2)_3(SeO_4)_5(NO_3) \cdot 3.5(H_2O)$ , (b)  $Na(C_8H_{10}NO_2)_7[(UO_2)_6(SO_4)_{10}] \cdot 3.5H_2O$ , (c)  $(C_4H_{12}N)_{14}[(UO_2)_{10}(SeO_4)_{17}(H_2O)]$ . (d–f) Nanotubes are cut into equal parts. The color indicates the chain type used in the construction of the NT. (g–i) Schematic representation of the tube. The inner diameters are defined as the distances between the opposite closest oxygen atoms.

The approach to the description of nanotubes as structural entities formed by layer scrolling is classic, and was applied for carbon NTs [45], transition-metal chalcogenides ( $MoS_2$ ,  $MoSe_2$ ,  $WS_2$ ,  $WSe_2$ ,  $NbS_2$  and  $NbSe_2$ ) [46], as well as oxides ( $TiO_2$ ,  $VO_x$ ,  $CuO$ ,  $Al_2O_3$ ,  $SiO_2$ , etc.) [47]. The topology of the smallest nanotubes (Figure 6a) corresponds to that of  $[(UO_2)_3(CrO_4)_5]^{4-}$  layers found in the structures of  $Mg_2[(UO_2)_3(CrO_4)_5] \cdot 17(H_2O)$  and  $Ca_2[(UO_2)_3(CrO_4)_5] \cdot 19(H_2O)$  [48]. The  $[(UO_2)_6(SO_4)_{10}]^{8-}$  nanotubes (Figure 6b) are produced from a similar layered archetype [44]. However, there are no layered “ancestors” for the  $[(UO_2)_{10}(SeO_4)_{17}(H_2O)]^{14-}$  nanotubes (Figure 6c), yet their local topology is similar to those of 3:5 layers, which were found, e.g., in the structure of  $Rb_4[(UO_2)_3(SeO_4)_5(H_2O)]$  [49].

If we dissect the  $[(UO_2)_3(SeO_4)_5]^{4-}$  tube, as shown in Figure 6a, the planar projection of the layer (Figure 6d) corresponds to the sequence of chains ... C1C2C1C1C2C1 ... Its repetition in a planar fashion ultimately leads to a layer with  $UO_2:TO_4 = 3:5$ .

The NT in  $\text{Na}(\text{C}_8\text{H}_{10}\text{NO}_2)_7[(\text{UO}_2)_6(\text{SO}_4)_{10}]\cdot 3.5\text{H}_2\text{O}$  [44] can be split (Figure 6b) into fundamental chains with the sequence of ...  $\text{C}'1\text{C}2\text{C}'1\text{C}'1\text{C}2\text{C}'1\text{C}'1\text{C}2\text{C}'1$  ... (Figure 6e). It is interesting to note that the sequence of chains is similar to those in  $\text{K}_5(\text{UO}_2)_3(\text{SeO}_4)_5(\text{NO}_3)\cdot 3.5(\text{H}_2\text{O})$ , but nine chains are required to build a tube.

The NTs in the structure of  $(\text{C}_4\text{H}_{12}\text{N})_{14}[(\text{UO}_2)_{10}(\text{SeO}_4)_{17}(\text{H}_2\text{O})]$  [42] can be dissected into ten chains (Figure 6i). In this case, the mutual arrangement of the polyhedra differs somewhat from the above discussed cases. Three chains ( $\text{C}'1$ ,  $\text{C}'1$ ,  $\text{C}2$ ) form a ribbon cut from the  $\text{UO}_2:\text{TO}_4 = 3:5$  layer.

In the topology of  $[(\text{UO}_2)_{10}(\text{SeO}_4)_{17}(\text{H}_2\text{O})]^{14-}$  nanotubules, the  $\text{C}'1\text{C}'1\text{C}2$  combination is repeated twice. Overall, the NT is formed from ten chains. Of the remaining four, two chains correspond to the  $\text{C}3$  described earlier, and two, to  $\text{C}4$ . The stacking sequence therefore is ...  $\text{C}4\text{C}3\text{C}'1\text{C}'1\text{C}2\text{C}4\text{C}3\text{C}'1\text{C}'1\text{C}2$  ... The  $\text{C}4$  are produced from  $\text{C}1$  if one link is broken between the tetrahedron and bipyramid in the  $(\text{UO}_2)_2(\text{TO}_4)_2$  cycle. Note the essential disorder [43] of some oxygen positions in the structure of  $(\text{C}_4\text{H}_{12}\text{N})_{14}[(\text{UO}_2)_{10}(\text{SeO}_4)_{17}(\text{H}_2\text{O})]$ . One may assume that in the idealized ordered version of the  $[(\text{UO}_2)_{10}(\text{SeO}_4)_{17}(\text{H}_2\text{O})]^{14-}$  NT, the topology of the  $\text{C}4$  chains would correspond to  $\text{C}1$ .

#### 4.2. The Flexibility of U-O-T Bridges

As follows from above, the inorganic uranyl NTs can be described as comprised of fundamental chains and, at a higher hierarchical level, derived from 3:5 layers or their fragments. The chain propagation axes are collinear to the axis of the NTs themselves. The NT in  $\text{K}_5[(\text{UO}_2)_3(\text{SeO}_4)_5](\text{NO}_3)3.5\text{H}_2\text{O}$  is comprised of six fundamental chains oriented parallel to the NT axis (Figure 6g). The scrolling of the precursor layer into the NT is probably enhanced by the flexibility of the U-O-T bridges. This essentially resembles a needle bearing wherein the rollers are replaced by the fundamental chains. The other NTs can be constructed in a similar way: the 7.4 Å-NT requires six chains (Figure 6g), 13.5 Å-NT, nine chains (Figure 6h) while ten are necessary for the 15.3 Å-NT (Figure 6i). To date, all known NTs differ merely by the number of fundamental chains they are comprised of.

It was noted earlier [14] that vertex-sharing between the  $\text{UO}_n$  and  $\text{TO}_4$  polyhedra results in the formation of a flexible “hinge” as the corresponding U-O-T angles can vary in a relatively broad range, providing the flexibility of the overall polyhedral backbone sufficient to compensate, for instance, the overall thermal expansion [50,51]. Yet, this mechanism seems not to contribute essentially to the formation of the NTs. The distribution of the U-O-T angles in the  $\text{UO}_2:\text{TO}_4 = 3:5$  layers (Figure 7a) covers a broad range of  $120^\circ$ – $165^\circ$ ; it has a nearly normal character with a maximum at  $135^\circ$ – $140^\circ$ . Almost the same is observed for the four NTs known to date (Figure 7b), the  $[(\text{UO}_2)_6(\text{SO}_4)_{10}]^{8-}$  NTs are the most flexible (U-O-S angles range from  $125^\circ$  to  $165^\circ$ ). The distribution is almost the same for  $[(\text{UO}_2)_3(\text{SeO}_4)_5]^{4-}$  and  $[(\text{UO}_2)_{10}(\text{SeO}_4)_{17}(\text{H}_2\text{O})]^{14-}$  NTs, the smallest one being evidently the most rigid.

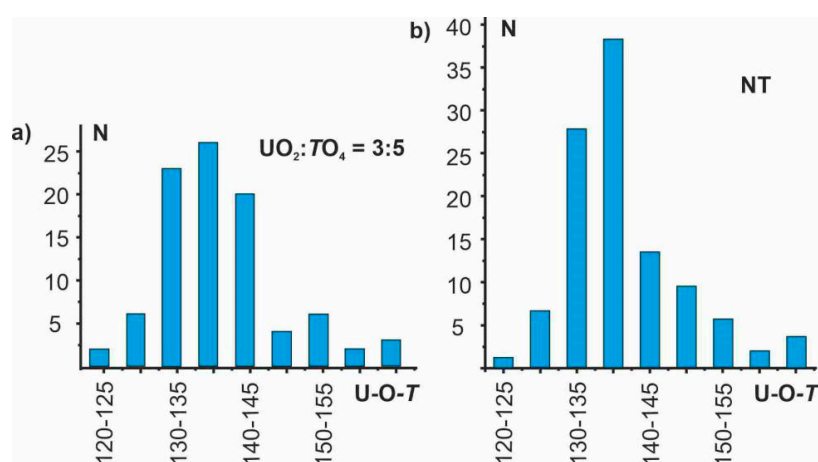
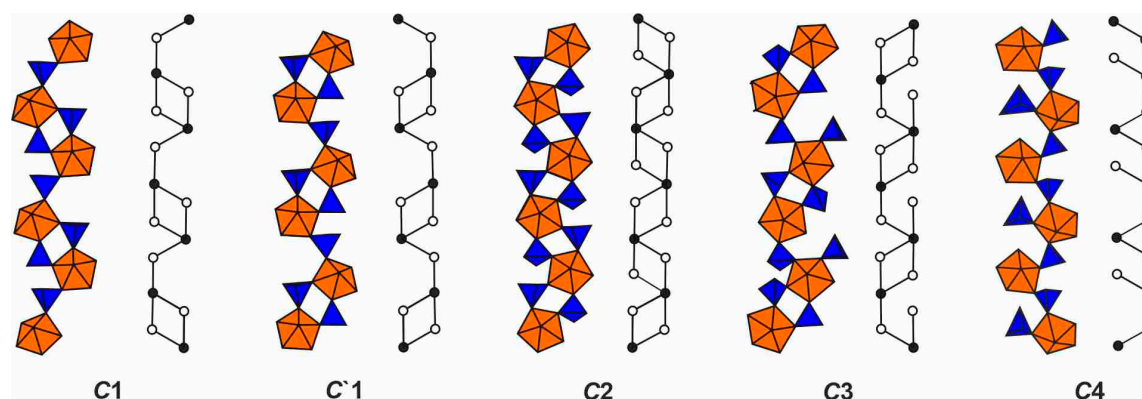


Figure 7. (a) The distribution of the U-O-T angles in known  $\text{UO}_2:\text{TO}_4 = 3:5$  layers and (b) in NT.

## 5. Conclusions

We described the synthesis and structure of the new uranyl molybdate templated by protonated isopropylamine molecules. The structure of modular  $[(\text{UO}_2)_3(\text{MoO}_4)_5]^{4-}$  layers in **1** represents a new isomer, not observed previously in uranyl molybdates.

Four different fundamental chains (C1, C'1, C2, C3) are sufficient for constructing any known layered topology with  $\text{UO}_2:\text{TO}_4 = 3:5$ , whereas five chains (C1, C'1, C2, C3, C4) are required for the known architectures of uranyl-based inorganic NTs (Figure 8).



**Figure 8.** Fundamental chains with edge-sharing polyhedral in the structures of known layered topologies with  $\text{UO}_2:\text{TO}_4 = 3:5$  and known complex NT derivatives.

The layers in the structure of **1** are topologically similar to the layers forming NTs in uranyl sulfates and selenates. In addition, the  $[(\text{UO}_2)_3(\text{MoO}_4)_5]^{4-}$  layers in **1** are identical to those in uranyl chromates. We can assume the formation of NTs with a similar topology in the structures of uranyl molybdates and uranyl chromates. The rarity of uranyl-based inorganic NTs, known to date, stems probably from the very narrow range of conditions which favor layer scrolling and which are only poorly understood to date.

While the majority of uranyl compounds adopt layered structures where the 1:2 and 2:3 layers are most common and exhibit rich topological diversity, these layers could not yet be scrolled. The formation of these layers requires only two types of fundamental chains [41], which is probably insufficient to form a NT. Out of ca. 1000 known uranyl compounds, only 10 contain the  $\text{UO}_2:\text{TO}_4 = 3:5$  layers, which can be scrolled, and just a handful of 4:7 and 5:8 representatives are known. Hence, formation conditions are very specific already for the “parental” layers, to say nothing about those for the scrolling and formation of nanotubules.

The results of the topological analysis of layered  $\text{UO}_2:\text{TO}_4 = 3:5$  architectures and derived nanotubules suggest that the latter may also form in uranyl molybdate systems.

**Author Contributions:** E.N. and O.S. designed the study, performed and interpreted single crystal X-ray diffraction experiments; D.C. performed synthesis; E.N., O.S. and D.C. wrote the paper; S.K. provided work in the radiochemical laboratory. All authors have read and agreed to the published version of the manuscript.

**Funding:** This work was financially supported by the Russian Science Foundation through the grant 16-17-10085.

**Acknowledgments:** Technical support by the SPbSU X-ray Diffraction and Microscopy and Microanalysis Resource Centers is gratefully acknowledged.

**Conflicts of Interest:** The authors declare no conflict of interest.

## References

1. Belova, L.N. *Zones of Oxidation of Hydrothermal Deposits of Uranium*; Nedra: Moscow, Russia, 1975; p. 158.
2. Hazen, R.M.; Ewing, R.C.; Sverjensky, D.A. Evolution of uranium and thorium minerals. *Am. Mineral.* **2009**, *94*, 1293–1311. [[CrossRef](#)]

3. Finch, R.J.; Murakami, T. Systematics and paragenesis of uranium minerals. In *Uranium: Mineralogy, Geochemistry and the Environment*; Burns, P.C., Finch, R.J., Eds.; Mineralogical Society of America: Chantilly, VA, USA, 1999; Reviews in Mineralogy; Volume 38, pp. 91–180.
4. Baker, R.J. Uranium minerals and their relevance to long term storage of nuclear fuels. *Coord. Chem. Rev.* **2014**, *266–267*, 123–136. [[CrossRef](#)]
5. Andrews, M.B.; Cahill, C.L. Uranyl bearing hybrid materials: Synthesis, speciation, and solid-state structures. *Chem. Rev.* **2013**, *113*, 1121–1136. [[CrossRef](#)] [[PubMed](#)]
6. Loiseau, T.; Mihalcea, I.; Henry, N.; Volkringer, C. The crystal chemistry of uranium carboxylates. *Coord. Chem. Rev.* **2014**, *266–267*, 69–109. [[CrossRef](#)]
7. Krivovichev, S.V. Structural crystallography of inorganic oxysalts. *Crystallogr. Rev.* **2009**, *15*, 279–281.
8. Krivovichev, S.V.; Plášil, J. Mineralogy and crystallography of uranium. In *Uranium: Cradle to Grave*; Mineralogical Association of Canada Short Course Series; Burns, P.C., Sigmon, G.E., Eds.; Mineralogical Association of Canada: Quebec, QC, Canada, 2013; pp. 15–120.
9. Kampf, A.R.; Plášil, J.; Kasatkin, A.V.; Marty, J. Belakovskite,  $\text{Na}_7(\text{UO}_2)(\text{SO}_4)_4(\text{SO}_3\text{OH})(\text{H}_2\text{O})_3$ , a new uranyl sulfate mineral from the Blue Lizard mine, San Juan County, Utah, USA. *Mineral. Mag.* **2014**, *78*, 639–649. [[CrossRef](#)]
10. Plášil, J.; Kampf, A.R.; Kasatkin, A.V.; Marty, J. Bluelizardite,  $\text{Na}_7(\text{UO}_2)(\text{SO}_4)_4\text{Cl}(\text{H}_2\text{O})_2$ , a new uranyl sulfate mineral from the Blue Lizard mine, San Juan County, Utah, USA. *J. Geosci. Czech.* **2014**, *59*, 145–158. [[CrossRef](#)]
11. Gurzhiy, V.V.; Plášil, J. Structural complexity of natural uranyl sulfates. *Acta Crystallogr. Sect. B* **2018**, *75*, 39–48. [[CrossRef](#)]
12. Kampf, A.R.; Plášil, J.; Kasatkin, A.V.; Marty, J. Bobcookite,  $\text{NaAl}(\text{UO}_2)_2(\text{SO}_4)_4 \cdot 18\text{H}_2\text{O}$  and wetherillite,  $\text{Na}_2\text{Mg}(\text{UO}_2)_2(\text{SO}_4)_4 \times 18\text{H}_2\text{O}$ , two new uranyl sulfate minerals from the Blue Lizard mine, San Juan County, Utah, USA. *Mineral. Mag.* **2015**, *79*, 695–714. [[CrossRef](#)]
13. Kampf, A.R.; Plášil, J.; Kasatkin, A.V.; Marty, J.; Čejka, J. Fermiite,  $\text{Na}_4(\text{UO}_2)(\text{SO}_4)_3 \cdot 3\text{H}_2\text{O}$  and oppeneimerite,  $\text{Na}_2(\text{UO}_2)(\text{SO}_4)_2 \cdot 3\text{H}_2\text{O}$ , two new uranyl sulfate minerals from the Blue Lizard mine, San Juan County, Utah, USA. *Mineral. Mag.* **2015**, *79*, 1123–1142. [[CrossRef](#)]
14. Krivovichev, S.V.; Burns, P.C.; Tananaev, I.G. (Eds.) *Structural Chemistry of Inorganic Actinide Compounds*; Elsevier: Amsterdam, The Netherlands, 2007; p. 494.
15. Kampf, A.R.; Sejkora, J.; Witzke, T.; Plášil, J.; Čejka, J.; Nash, B.P.; Marty, J. Rietveldite,  $\text{Fe}(\text{UO}_2)(\text{SO}_4)_2(\text{H}_2\text{O})_5$ , a new uranyl sulfate mineral from Giveaway-Simplot mine (Utah, USA), Willi Agatz mine (Saxony, Germany) and Jáchymov (Czech Republic). *J. Geosci. Czech.* **2017**, *62*, 107–120. [[CrossRef](#)]
16. Plášil, J.; Hloušek, J.; Kasatkin, A.V.; Novak, M.; Čejka, J.; Lapčák, L. Svornostite,  $\text{K}_2\text{Mg}[(\text{UO}_2)(\text{SO}_4)_2]_2 \cdot 8\text{H}_2\text{O}$ , a new uranyl sulfate mineral from Jáchymov, Czech Republic. *J. Geosci. Czech.* **2015**, *60*, 113–121. [[CrossRef](#)]
17. Plášil, J.; Kampf, A.R.; Kasatkin, A.V.; Marty, J.; Skoda, R.; Silva, S.; Čejka, K. Meisserite,  $\text{Na}_5(\text{UO}_2)(\text{SO}_4)_3(\text{SO}_3\text{OH})(\text{H}_2\text{O})$ , a new uranyl sulfate mineral from the Blue Lizard mine, San Juan County, Utah, USA. *Mineral. Mag.* **2013**, *77*, 2975–2988. [[CrossRef](#)]
18. Nazarchuk, E.V.; Charkin, D.O.; Siidra, O.I.; Gurzhiy, V.V. Crystal-chemical features of U(VI) compounds with inorganic complexes derived from  $[(\text{UO}_2)(\text{TO}_4)(\text{H}_2\text{O})_n]$ ,  $T = \text{S, Cr, Se}$ : Synthesis and crystal structures of two new uranyl sulfates. *Radiochemistry* **2018**, *60*, 345–351. [[CrossRef](#)]
19. Kampf, A.R.; Plášil, J.; Kasatkin, A.V.; Marty, J.; Čejka, J.; Lapčák, L. Shumwayite,  $[(\text{UO}_2)(\text{SO}_4)(\text{H}_2\text{O})_2]_2 \cdot \text{H}_2\text{O}$ , a new uranyl sulfate mineral from Red Canyon, San Juan County, Utah, USA. *Mineral. Mag.* **2017**, *81*, 273–285. [[CrossRef](#)]
20. Pushcharovskii, D.Y.; Rastsvetaeva, R.K.; Sarp, H. Crystal structure of deloryite,  $\text{Cu}_4(\text{UO}_2)(\text{Mo}_2\text{O}_8)(\text{OH})_6$ . *J. Alloys Compd.* **1996**, *239*, 23–26. [[CrossRef](#)]
21. Mereiter, K. The crystal structure of walpurgite,  $(\text{UO}_2)\text{Bi}_4\text{O}_4(\text{AsO}_4)_2 \cdot 2\text{H}_2\text{O}$ . *Tschermaks Mineral. Petrogr. Mitt.* **1982**, *30*, 129–139. [[CrossRef](#)]
22. Krause, W.; Effenberger, H.; Brandstaetter, F. Orthowalpurgite,  $(\text{UO}_2)\text{Bi}_4\text{O}_4(\text{AsO}_4)_2 \cdot 2(\text{H}_2\text{O})$ , a new mineral from the Black Forest, Germany. *Eur. J. Inorg. Mineral.* **1995**, *7*, 1313–1324.
23. Locock, A.J.; Burns, P.C. The crystal structure of synthetic autunite,  $\text{Ca}((\text{UO}_2)(\text{PO}_4))_2(\text{H}_2\text{O})_{11}$ . *Am. Mineral.* **2003**, *88*, 240–244. [[CrossRef](#)]

24. Kampf, A.R.; Plášil, J.; Kasatkin, A.V.; Nash, B.P.; Marty, J. Magnesioleydetite and straßmannite, two new uranyl sulfate minerals with sheet structures from Red Canyon, Utah. *Mineral. Mag.* **2019**, *83*, 349–360. [[CrossRef](#)]
25. Alekseev, E.V.; Suleimanov, E.V.; Chuprunov, E.V.; Marychev, M.O.; Ivanov, V.; Fukin, G.K. Crystal structures and nonlinear optical properties of  $K_2UO_2(SO_4)_2 \cdot 2H_2O$  compound at 293K. *Crystallogr. Rep.* **2006**, *51*, 29–33. [[CrossRef](#)]
26. Plášil, J.; Kasatkin, A.V.; Skoda, R.; Novak, M.; Kallistova, A.; Dusek, M.; Skala, R.; Fejfarova, K.; Cejka, J.; Meisser, N.; et al. Leydetite,  $Fe(UO_2)(SO_4)_2(H_2O)_{11}$ , a new uranyl sulfate mineral from Mas d'Alary, Lodeve, France. *Mineral. Mag.* **2013**, *77*, 429–441. [[CrossRef](#)]
27. Pekov, I.V.; Krivovichev, S.V.; Yapaskurt, V.O.; Chukanov, N.V.; Belakovskiy, D.I. Beshtautite,  $(NH_4)_2(UO_2)(SO_4)_2 \cdot 2(H_2O)$ , a new mineral from Mount Beshtau, Northern Caucasus, Russia. *Am. Mineral.* **2014**, *99*, 1783–1787. [[CrossRef](#)]
28. Márquez-Zavalía, M.F.; Galliski, M.A. Goldichite of fumarolic origin from the Santa 1062 Bárbara mine, Jujuy, Northwestern Argentina. *Can. Mineral.* **1995**, *33*, 1059–1062.
29. Ling, J.; Sigmon, G.E.; Ward, M.; Roback, N.; Burns, P.C. Syntheses, structures, and IR spectroscopic characterization of new uranyl sulfate/selenate 1D-chain, 2D-sheet and 3D-framework. *Z. Kristallogr.* **2010**, *225*, 230–239. [[CrossRef](#)]
30. Doran, M.B.; Norquist, A.J.; O'Hare, D. Exploration of composition space in templated uranium sulfates. *Inorg. Chem.* **2003**, *42*, 6989–6995. [[CrossRef](#)]
31. Norquist, A.J.; Doran, M.B.; Thomas, P.M.; O'Hare, D. Structural diversity in organically templated uranium sulfates. *Dalton Trans.* **2003**, *6*, 1168–1175. [[CrossRef](#)]
32. Siidra, O.I.; Nazarchuk, E.V.; Suknotova, A.N.; Kayukov, R.A.; Krivovichev, S.V. Cr(VI) trioxide as a starting material for the synthesis of novel zero-, one-, and two-dimensional uranyl dichromates and chromate-dichromates. *Inorg. Chem.* **2013**, *52*, 4729–4735. [[CrossRef](#)]
33. Gagné, O.C.; Hawthorne, F.C. Comprehensive derivation of bond-valence parameters for ion pairs involving oxygen. *Acta Cryst.* **2015**, *B71*, 561–578. [[CrossRef](#)]
34. Halasyamani, P.S.; Francis, R.J.; Walker, S.M.; O'Hare, D. New layered uranium(VI) molybdates: syntheses and structures of  $(NH_3(CH_2)_3NH_3)(H_3O)_2(UO_2)_3(MoO_4)_5$ ,  $C(NH_2)_3(UO_2)(OH)(MoO_4)$ ,  $(C_4H_{12}N_2)(UO_2)(MoO_4)_2$  and  $(C_5H_{14}N_2)(UO_2)(MoO_4)_2 \cdot H_2O$ . *Inorg. Chem.* **1999**, *38*, 271–279. [[CrossRef](#)]
35. Krivovichev, S.V.; Tananaev, I.G.; Myasoedov, B.F. Geometric isomerism of layered complexes of uranyl selenates: Synthesis and structure of  $(H_3O)[C_5H_{14}N]_2[(UO_2)_3(SeO_4)_4(HSeO_4)(H_2O)]$  and  $(H_3O)[C_5H_{14}N]_2[(UO_2)_3(SeO_4)_4(HSeO_4)(H_2O)](H_2O)$ . *Radiochemistry* **2006**, *48*, 552–560. [[CrossRef](#)]
36. Krivovichev, S.V.; Burns, P.C. Crystal chemistry of K uranyl chromates: Crystal structures of  $K_5[(UO_2)(CrO_4)_3](NO_3)(H_2O)_3$ ,  $K_4[(UO_2)_3(CrO_4)_5](H_2O)_7$  and  $K_2[(UO_2)_2(CrO_4)_3](H_2O)_6$ . *Z. Kristallogr. Cryst. Mater.* **2003**, *218*, 725–730.
37. Moore, P.B. Laueite, pseudolaueite, stewartite and metavauxite: A study in combinatorial polymorphism. *Neu. Jb. Mineral. Abh.* **1975**, *123*, 148–159.
38. Krivovichev, S.V.; Tananaev, I.G. Microscopic model of crystal genesis from aqueous solution of uranyl selenates. *J. Sib. Fed. Uni. Chem.* **2009**, *2*, 133–149.
39. Krivovichev, S.V.; Burns, P.C. The modular structure of the novel uranyl sulfate sheet in  $[Co(H_2O)_6]_3[(UO_2)_5(SO_4)_8(H_2O)](H_2O)_5$ . *J. Geosci. Czech.* **2014**, *59*, 135–143. [[CrossRef](#)]
40. Nazarchuk, E.V.; Siidra, O.I.; Charkin, D.O. Specific features of the crystal chemistry of layered uranyl compounds with the ratio  $UO_2:TO_4 = 5:8$  ( $T = S^{6+}, Cr^{6+}, Se^{6+}, Mo^{6+}$ ). *Radiochemistry* **2018**, *60*, 352–361. [[CrossRef](#)]
41. Nazarchuk, E.V.; Charkin, D.O.; Kozlov, D.V.; Siidra, O.I.; Kalmykov, S.N. Topological analysis of the layered uranyl compounds bearing slabs with  $UO_2:TO_4$  ratio of 2:3. *Radiochim. Acta.* **2020**, *108*, 249–260. [[CrossRef](#)]
42. Krivovichev, S.V.; Tananaev, I.G.; Kahlenberg, V.; Kaindl, R.; Myasoedov, B.F. Synthesis, structure, and properties of inorganic nanotubes based on uranyl selenates. *Radiochemistry* **2005**, *47*, 525–536. [[CrossRef](#)]
43. Alekseev, E.V.; Krivovichev, S.V.; Depmeier, W. A crown ether as template for microporous and nanostructured uranium compounds. *Angew. Chem. Int. Ed.* **2008**, *47*, 549–551. [[CrossRef](#)]
44. Siidra, O.I.; Nazarchuk, E.V.; Charkin, D.O.; Chukanov, N.V.; Depmeier, W.; Bocharov, S.N.; Sharikov, M.I. Uranyl sulfate nanotubules templated by N-phenylglycine. *Nanomaterials* **2018**, *8*, 216. [[CrossRef](#)]
45. Iijima, S. Helical microtubules of graphitic carbon. *Nature* **1991**, *354*, 56–58. [[CrossRef](#)]

46. Tenne, R.; Margulis, L.; Genut, M.; Hodes, G. Polyhedral and cylindrical structures of tungsten disulphide. *Nature* **1992**, *360*, 444–446. [[CrossRef](#)]
47. Imai, H.; Matsuta, M.; Shimizu, K.; Hirashima, H.; Negishi, N. Preparation of TiO<sub>2</sub> fibers with well-organized structures. *J. Mater. Chem.* **2000**, *10*, 2005–2006. [[CrossRef](#)]
48. Krivovichev, S.V.; Burns, P.C. Geometrical isomerism in uranyl chromates II. Crystal structures of Mg<sub>2</sub>[(UO<sub>2</sub>)<sub>3</sub>(CrO<sub>4</sub>)<sub>5</sub>] 17(H<sub>2</sub>O) and Ca<sub>2</sub>[(UO<sub>2</sub>)<sub>3</sub>(CrO<sub>4</sub>)<sub>5</sub>] 19(H<sub>2</sub>O). *Z. Crystallogr.* **2003**, *218*, 683–690. [[CrossRef](#)]
49. Krivovichev, S.V.; Kahlenberg, V. Structural diversity of sheets in rubidium uranyl oxoselenates: Synthesis and crystal structures of Rb<sub>2</sub>((UO<sub>2</sub>)(SeO<sub>4</sub>)<sub>2</sub>(H<sub>2</sub>O))(H<sub>2</sub>O), Rb<sub>2</sub>((UO<sub>2</sub>)<sub>2</sub>(SeO<sub>4</sub>)<sub>3</sub>(H<sub>2</sub>O)<sub>2</sub>)(H<sub>2</sub>O)<sub>4</sub> and Rb<sub>4</sub>((UO<sub>2</sub>)<sub>3</sub>(SeO<sub>4</sub>)<sub>5</sub>(H<sub>2</sub>O)). *Z. Anorg. Allg. Chem.* **2005**, *631*, 739–744. [[CrossRef](#)]
50. Nazarchuk, E.V.; Krivovichev, S.V.; Filatov, S.K. Phase transitions and high-temperature crystal chemistry of polymorphous modifications of Cs<sub>2</sub>(UO<sub>2</sub>)<sub>2</sub>(MoO<sub>4</sub>). *Radiochemistry* **2004**, *46*, 438–440. [[CrossRef](#)]
51. Siidra, O.I.; Nazarchuk, E.V.; Kayukov, R.A.; Bubnova, R.S.; Krivovichev, S.V. Cr<sup>VI</sup>–Cr<sup>V</sup> transition in Uranyl Chromium compounds: Synthesis and high-temperature X-ray diffraction study of Cs<sub>2</sub>[(UO<sub>2</sub>)<sub>2</sub>(CrO<sub>4</sub>)<sub>3</sub>]. *Z. Anorg. Allg. Chem.* **2013**, *639*, 2302–2306. [[CrossRef](#)]



© 2020 by the authors. Licensee MDPI, Basel, Switzerland. This article is an open access article distributed under the terms and conditions of the Creative Commons Attribution (CC BY) license (<http://creativecommons.org/licenses/by/4.0/>).